Genetic tracing of hepatocytes in liver homeostasis, injury, and regeneration

Received for publication, February 16, 2017, and in revised form, March 27, 2017 Published, Papers in Press, April 4, 2017, DOI 10.1074/jbc.M117.782029

Yue Wang[‡§1], XiuZhen Huang[‡§1], Lingjuan He[‡§], Wenjuan Pu[‡§], Yan Li[‡§], Qiaozhen Liu[‡§], Yi Li[‡§], Libo Zhang[‡§], Wei Yu[‡§], Huan Zhao[‡§], Yingqun Zhou[¶2], and Bin Zhou[‡§‖3]**

*From [‡]The State Key Laboratory of Cell Biology, CAS Center for Excellence in Molecular Cell Science, Shanghai Institute of Biochemistry and Cell Biology, Chinese Academy of Sciences, University of Chinese Academy of Sciences, Shanghai 200031, China, the [§]Key Laboratory of Nutrition and Metabolism, Institute for Nutritional Sciences, Shanghai Institutes for Biological Sciences, Chinese Academy of Sciences, University of Chinese Academy of Sciences, Shanghai 200031, China, the [¶]Department of Gastroenterology, Shanghai 10th People's Hospital, Tongji University School of Medicine, Shanghai 200072, China, the [‖]Key Laboratory of Regenerative Medicine of Ministry of Education, Institute of Aging and Regenerative Medicine, Jinan University, Guangzhou 510632, China, and the **School of Life Science and Technology, ShanghaiTech University, Shanghai 201210, China*

Edited by Jeffrey E. Pessin

The liver possesses a remarkable capacity to regenerate after damage. There is a heated debate on the origin of new hepatocytes after injuries in adult liver. Hepatic stem/progenitor cells have been proposed to produce functional hepatocytes after injury. Recent studies have argued against this model and suggested that pre-existing hepatocytes, rather than stem cells, contribute new hepatocytes. This hepatocyte-to-hepatocyte model is mainly based on labeling of hepatocytes with Cre-recombinase delivered by the adeno-associated virus. However, the impact of virus infection on cell fate determination, consistency of infection efficiency, and duration of Cre-virus in hepatocytes remain confounding factors that interfere with the data interpretation. Here, we generated a new genetic tool *Alb-DreER* to label almost all hepatocytes (>99.5%) and track their contribution to different cell lineages in the liver. By "pulse-and-chase" strategy, we found that pre-existing hepatocytes labeled by *Alb-DreER* contribute to almost all hepatocytes during normal homeostasis and after liver injury. Virtually all hepatocytes in the injured liver are descendants of pre-existing hepatocytes through self-expansion. We concluded that stem cell differentiation is unlikely to be responsible for the generation of a substantial number of new hepatocytes in adult liver. Our study also provides a new mouse tool for more precise *in vivo* genetic study of hepatocytes in the field.

Adult mammalian tissues rely on diverse mechanisms to maintain function and mass. It is well established that organs can maintain homeostasis via either cellular replication or differentiation from stem cells. The liver has a remarkable capacity for regeneration (1). It has been reported that liver regeneration can be driven not only by hepatocytes but also by facultative stem cells under certain injury conditions (2). During chronic and acute injuries, differentiated hepatocytes reenter the cell cycle, proliferate, and replenish the lost tissue. Based on *in vitro* and *in vivo* experiments, bipotential hepatobiliary progenitors (often called oval cells) were proposed as the main source of new hepatocytes and ductal cells under conditions that interfere with hepatocyte proliferation (3–6). Leclercq *et al.* (3) performed lineage tracing experiments using *OPN-iCreER^{T2};Rosa26R^{YFP}* mice to show that liver progenitor cells or biliary cells terminally differentiate into functional hepatocytes in mice with liver injury. Clevers and co-workers (4) used *Lgr5-IRES-CreER^{T2};Rosa26-lacZ* mice to find that Lgr5-lacZ is not expressed in healthy adult liver; however, small Lgr5-LacZ^{+} cells appear near bile ducts upon damage, coinciding with robust activation of Wnt signaling. By lineage tracing, they demonstrated that these Lgr5-LacZ^{+} cells generate hepatocytes and biliary duct cells during the repair phase, indicating that Lgr5^{+} cells as bipotent liver progenitors (4). Recent studies showed that Sox9^{+} biphenotypic hepatocytes were derived from mature hepatocytes, and some of them were incorporated into ductular structures, whereas they efficiently differentiate to functional hepatocytes (5). Therefore, biphenotypic hepatocytes not only terminally convert to cholangiocytes but also differentiate back to mature hepatocytes. Mature epithelial cells can show plasticity upon severe injuries and contribute to regeneration (5). In addition, activation of Notch is sufficient to reprogram hepatocytes into biliary epithelial cells (6).

However, recent studies using genetic lineage-tracing experiments suggested that oval cells contribute minimally to hepa-

This work was supported by the National Science Foundation of China (91639302, 31625019, 91339104, 31271552, 31222038, 31571503, 31501172, 31601168, and 81300340), Ministry of Science and Technology (2013CB945302 and 2016YFC1300600), Strategic Priority Research Program of the Chinese Academy of Sciences (CAS, XDB19000000), Youth Innovation Promotion Association of CAS (2015218), Key Project of Frontier Sciences of CAS (QYZDB-SSW-SMC003), International Cooperation Fund of CAS, Shanghai Zhangjiang Stem Cell Research Project (ZJ2014-ZD-002), Shanghai Science and Technology Commission (14JC1407400 and 16DZ2280800), Shanghai Yangfan Project (15YF1414000) and Rising-Star Program (15QA1404300), China Postdoctoral Science Foundation (2015M581669, 2016T90387, and 2016LH0042), President Fund of Shanghai Institutes for Biological Sciences (SIBS), and an AstraZeneca and Sanofi-SIBS Fellowship. The authors declare that they have no conflicts of interest with the contents of this article.

[1] Both authors contributed equally to this work.
[2] To whom correspondence may be addressed: 301 Yanchang Rd., Dept. of Gastroenterology, Shanghai Tenth People's Hospital, Tongji University School of Medicine, Shanghai 200072, China. Tel.: 86-21-66302535; Fax: 86-21-66301051; E-mail: yqzh02@163.com.
[3] To whom correspondence may be addressed: 320 Yueyang Rd., Life Science Research Bld. A-2112, Shanghai 200031, China. Tel.: 86-21-54920974; Fax: 86-21-54920974; E-mail: zhoubin@sibs.ac.cn.

© 2017 by The American Society for Biochemistry and Molecular Biology, Inc. Published in the U.S.A.

tocyte restoration (7–10). Pau Sancho-Bru and co-workers (7) used a tamoxifen-inducible Hnf1β CreER;R26R$^{Yfp/LacZ}$ mouse to lineage trace Hnf1β^+ biliary duct cells and to assess their contribution to liver progenitor cell expansion and hepatocyte generation. They demonstrated no contribution of Hnf1β^+ cells to hepatocyte during liver homeostasis in healthy mice or after loss of liver mass. After acute acetaminophen or CCl4 (carbon tetrachloride) injury, no contribution of Hnf1β^+ cells to hepatocytes was detected (7). Although no contribution was observed after 3,5-diethoxycarbonyl-1,4-dihydrocollidine (DDC)[4]-diet treatment, mice fed with a choline-deficient ethionine-supplemented (CDE)-diet showed a small population of hepatocytes derived from Hnf1β^+ cells that were expanded to just 1.86% of total hepatocytes after injury recovery (7). Willenbring and co-workers (8) injected into reporter mice an adeno-associated viral vector expressing Cre from the transthyretin promoter (AAV8-Ttr-Cre) that afforded specific and efficient reporter gene activation in hepatocytes but did not label BECs, stellate cells, macrophages, or endothelial cells in livers. In contrast to previous studies, they failed to detect hepatocytes derived from biliary epithelial cells or mesenchymal liver cells beyond a negligible frequency (8). In fact, they failed to detect hepatocytes that were not derived from pre-existing hepatocytes. Their findings argue against liver stem cells or other non-hepatocyte cell types, providing a backup system for hepatocyte regeneration in chronic liver injury models (8). Grompe and co-workers (9) also used clonal tracing strategy to further research the liver progenitors issue. The biliary or nonparenchymal compartments were traced en masse, which precludes the identification of clonal relationships between hepatocytes and ductal progenitors. It has been reported that tamoxifen can induce "ectopic" expression of ductal markers in hepatocytes (11), and biliary transcription factors are expressed in normal hepatocytes (12). Grompe and co-workers suggested that a clonal labeling strategy is needed to directly identify the origin of hepatocyte precursor cells in liver repair. They used Sox9-CreER^{T2};R26R-Confetti multicolor stochastic reporter mouse to establish the tamoxifen dose suitable for clonal labeling. Their data showed that bipotential hepatic progenitors of Sox9$^+$ ductal origin do not contribute significantly to hepatocyte replacement, and hepatocytes themselves are the predominant source of new parenchymal cells (9). Similarly, Stanger and co-workers (10) team used genetic and nucleoside analog-based tools to mark and track the origin and contribution of various cell populations to liver regeneration. They concluded that there is virtually all new hepatocytes come from pre-existing hepatocytes.

The genetic lineage tracing of hepatocytes in previous works mainly depends on the Cre-expressing adeno-associated virus (AAV8) that specifically targets hepatocytes. Due to the unknown effect of excessive virus on the hepatocyte proliferation and also the duration of the Cre-expressing virus in hepatocytes, the virus-mediated lineage-tracing data should be interpreted with cautions. We, therefore, generated a hepatocyte-inducible tracing mouse line and directly labeled hepatocytes by tamoxifen induction and traced the change of hepatocyte-labeling efficiency under multiple liver injury conditions. Our studies demonstrated that hepatocytes, not other kinds of liver cells, act as the main source for hepatocyte replenishment and regeneration in adult liver after different types of injury.

Results

Generation and characterization of Alb-DreER mouse line

Albumin is synthesized in the liver and functions primarily as a carrier protein for steroids, fatty acids, and thyroid hormones and plays a role in stabilizing extracellular fluid volume (13, 14). During liver development, albumin is specifically expressed in liver hepatoblasts (progenitors of both biliary epithelial cells (BECs) and hepatocytes). Its expression is restricted to mature hepatocytes in adult stage (15). We, therefore, utilize the Alb gene to generate a genetic tool for inducible lineage tracing of hepatocytes. We first generated *Alb-DreER* by knocking a cDNA encoding DreER^{T2} into the last coding exon of Alb using CRISPR/Cas9 through homologous recombination. This knock-in strategy leads to simultaneous expression of DreER and endogenous albumin. Dre is a site-specific recombinase that targets the rox site, and similar to Cre-loxP, Dre-rox recombination has also been used for genetic lineage tracing (16–18). By crossing *Alb-DreER* with the *R26-RSR-tdTomato* reporter line (16, 17), we generated *Alb-DreER;R26-RSR-tdTomato* mice and treated them with tamoxifen for induction of Dre-rox recombination (Fig. 1*A*). Dre-rox recombination will remove rox-flanked transcriptional Stop cassette, leading to tdTomato expression and cell labeling (Fig. 1*B*). This genetic labeling is heritable and irreversible so that all the descendants of Alb-expressing cells will permanently express the genetic marker tdTomato. In adult *Alb-DreER;R26-RSR-tdTomato* mice collected 4 days after tamoxifen induction, we observed *Alb-DreER* efficiently labeled cells in liver (Fig. 1*C*). Immunostaining for the genetic marker tdTomato, the biliary epithelial cell marker CK19, and hepatocyte marker HNF4α on liver sections showed that *Alb-DreER* labeled almost all hepatocytes but not BECs (Fig. 1*D*). To detect the leakiness of DreER, we collected the liver of *Alb-DreER;R26-RSR-tdTomato* mice that did not receive tamoxifen. Immunostaining for tdTomato and HNF4α on liver sections shows sparse tdTomato$^+$ hepatocytes (Fig. 1*D*), indicating that a high labeling percentage of hepatocytes after tamoxifen induction is unlikely due to leakiness of DreER. Immunostaining for tdTomato and other non-hepatocyte lineage markers showed that *Alb-DreER* did not label Sox9$^+$ or EpCAM$^+$ biliary epithelia cells, Desmin$^+$ hepatic stellate cells, PDGFRα^+ fibroblasts, VE-cadherin$^+$ vascular endothelial cells, or aSMA$^+$ smooth muscle cells in the liver (Fig. 1*E*). Quantification data showed that 99.64 $\pm$ 0.15% of hepatocytes were tdTomato$^+$ at 1 week after tamoxifen treatment. At 6 weeks after tamoxifen treatment, the percentage of tdTomato$^+$ hepatocytes remained similar to that of 1 week (99.54 $\pm$ 0.19%, $n = 4$) (Fig. 1*F*). Taken together, our results demonstrated that *Alb-DreER* efficiently and specifically labels

[4] The abbreviations used are: DDC, 3,5-diethoxycarbonyl-1,4-dihydrocollidine; BEC, biliary epithelial cell; CDE, choline-deficient ethionine-supplemented; ANIT, α-naphthyl-isothiocyanate; PHx, partial hepatectomy; BDL, bile-duct ligation; AAV, adeno-associated virus; VE-cadherin, vascular endothelial cadherin.

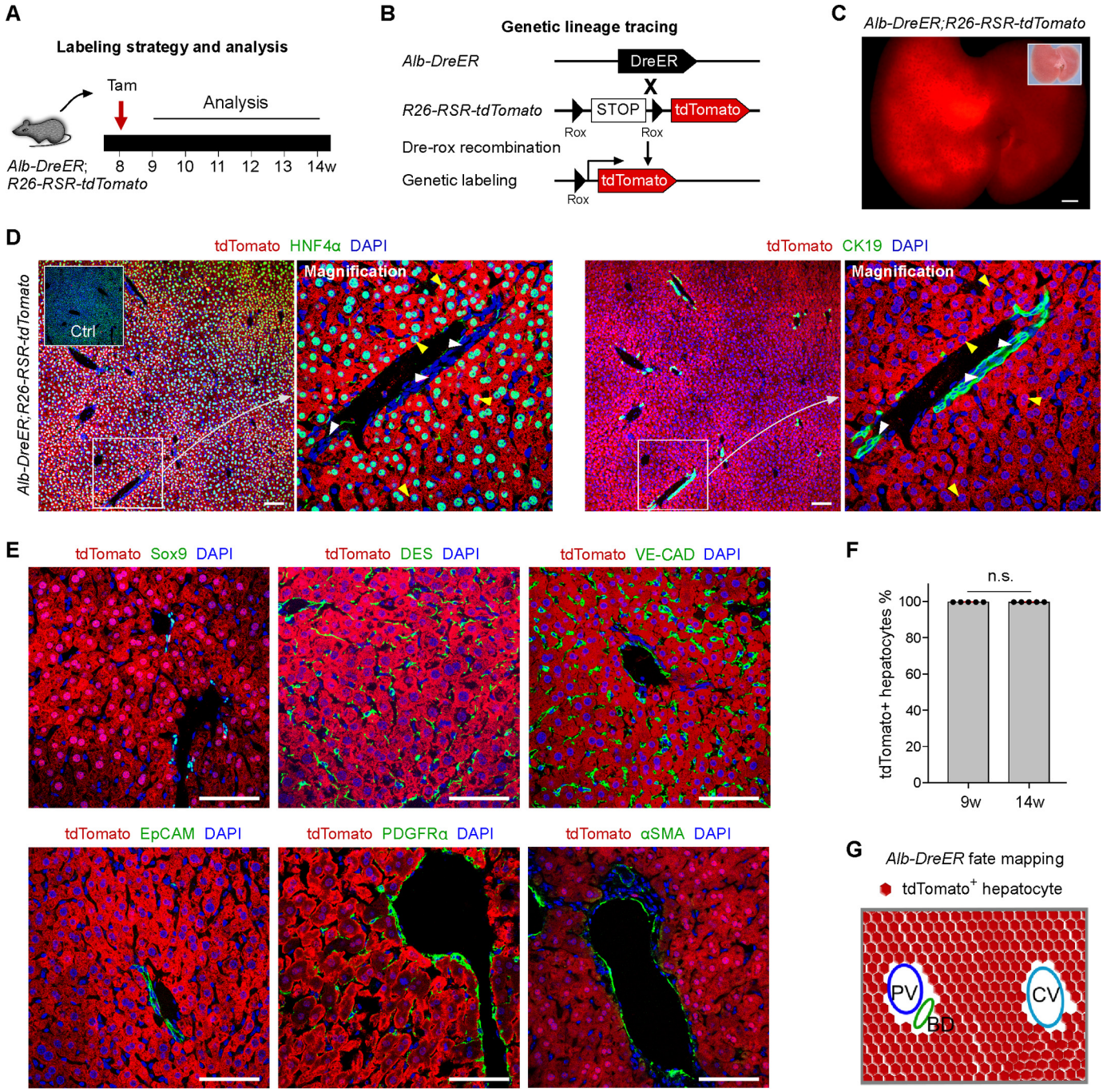

Figure 1. Alb-DreER specifically and efficiently labeled adult hepatocytes. *A*, schematic showing experimental strategy for lineage tracing of Alb+ cells. *B*, genetic lineage tracing strategy by Dre-Rox recombination in Alb+ hepatocytes. *C*, whole-mount fluorescence view of adult liver from 9-week-old *Alb-DreER;R26-RSR-tdTomato* mice. Tamoxifen was induced at 8 weeks. The *inset* indicates the bright-field image of the same liver. *D*, immunostaining for tdTomato, CK19, and HNF4α on liver sections shows Alb-DreER labeled almost all hepatocytes (*yellow arrowheads*) but no ductal cells (*white arrowheads*). The *inset* indicates same the staining on the liver section of *Alb-DreER;R26-RSR-tdTomato* mouse without tamoxifen treatment. *E*, immunostaining for tdTomato and other lineage markers shows tdTomato+ cells (*red*) are not SOX9+, EpCAM+, DES+, PDGFRα+, VE-CAD+, or αSMA+ cells (*green*). *F*, quantification of labeled hepatocytes at 9- or 14-week-old mice. *n.s.*, non-significant; $n = 5$. *G*, schematic image showing labeling of hepatocytes by Alb-DreER. *Scale bars*, 1 mm in *C* and 100 μm in *D* and *E*. *Error bars*, S.E.

hepatocytes in adult mouse liver (Fig. 1*G*), and this genetic tool could be utilized to study the cell fate of hepatocytes after liver injuries.

Hepatocytes are derived from pre-existing hepatocytes after CCl4 injury

To test whether hepatocytes arise from progenitor cells after chronic liver injury, we labeled almost all hepatocytes using *Alb-DreER;Rosa26-RSR-tdTomato* mice to determine if most hepatocytes after injury are derived from pre-existing labeled hepatocytes. By using and-chase strategy, we reasoned that if unlabeled hepatic progenitor cells contribute to new hepatocytes after injury, these new hepatocytes would be unlabeled. If the number of unlabeled hepatocytes from progenitor cells is substantial, it would significantly dilute the labeling percentage of hepatocytes. If their contribution is negligible, we may not

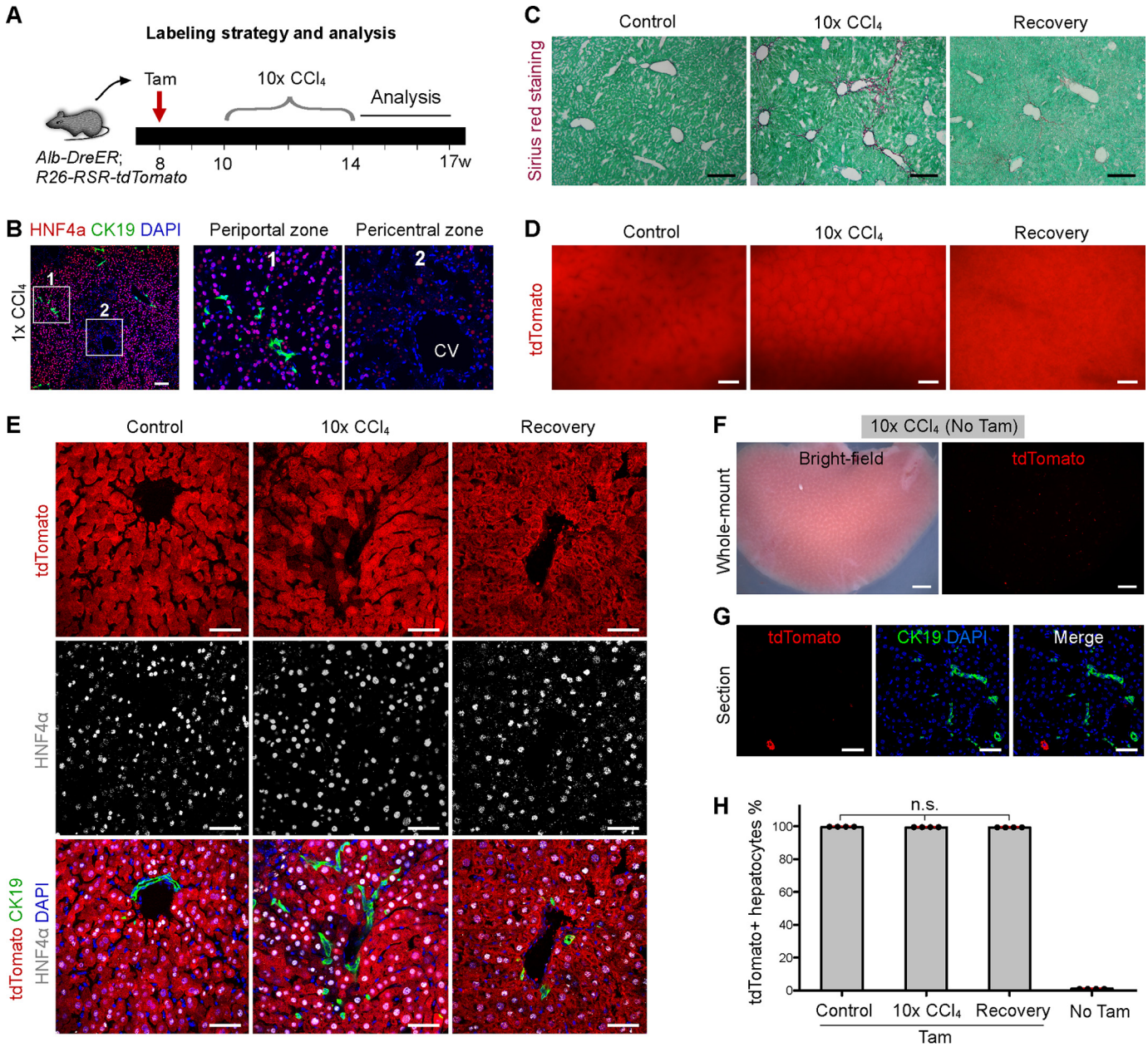

Figure 2. New hepatocytes were derived from pre-existing hepatocytes after CCl4 injury. *A*, schematic figure showing experimental strategy for tamoxifen treatment (*Tam*) and tissue analysis. *B*, immunostaining for HNF4α and CK19 on liver sections collected from mouse at 2 days after one-dose CCl4 treatment showed that most pericentral hepatocytes are dead. *CV*, central vein; *1* and *2* are magnified images of *boxed regions*. C, Sirius red staining of liver sections from oil (*Control*), chronic CCl4-treated mice (10× CCl4), or after recovery (3 weeks after last CCl4 treatment). *D*, whole-mount fluorescence view of *Alb-DreER;R26-RSR-tdTomato* liver samples. *E*, immunostaining for tdTomato, CK19, and HNF4α on liver sections shows almost all hepatocytes in injured and recovered groups are tdTomato+. *F*, whole-mount bright-field or fluorescence view of CCl4 injured livers from *Alb-DreER;R26-RSR-tdTomato* mice without tamoxifen treatment (*No Tam*). *G*, immunostaining for tdTomato and CK19 on liver section shows sparse tdTomato+ hepatocytes. *H*, quantification of tdTomato+ hepatocytes in different groups. *n.s.*, non-significant; $n = 4$. *Scale bars*,100 μm in *B*, *E*, and *G*; 200 μm in *C*; 500 μm in *D*; 1 mm in *F*. *Error bars*, S.E.

detect significant dilution of the labeled hepatocytes. We could, therefore, infer from these data that new hepatocytes are mainly derived from pre-existing hepatocytes or hepatic precursor cells.

Next, we used this pulse-and-chase strategy to analyze the percentage of labeled hepatocytes during the liver regeneration after different types of injury models. The *Alb-DreER;Rosa26-RSR-tdTomato* mice were treated with CCl4 to induce chronic injury (Fig. 2*A*). Shortly after CCl4 treatment, we found a significant loss of hepatocytes in the pericentral region compared with fairly normal condition of hepatocytes in the periportal region (Fig. 2*B*). During chronic injury, periportal hepatocytes will migrate and compensate for the loss of pericentral hepatocytes (19). Sirius red staining confirmed a significant fibrosis in CCl4-treated liver compared with oil-treated liver (*Control*) or liver collected at 3-weeks' recovery after injury (*Recovery*) (Fig. 2*C*). Whole-mount epifluorescence view of livers from different groups shows no significant dilution of fluorescence signal after liver injury (Fig. 2*D*). Immunostaining for tdTomato, CK19, and HNF4α showed that almost all hepatocytes in the injured and control livers were tdTomato$^+$ (Fig. 2*E*). By CCl4 treatment, we did not detect any BECs derived from tdTomato$^+$

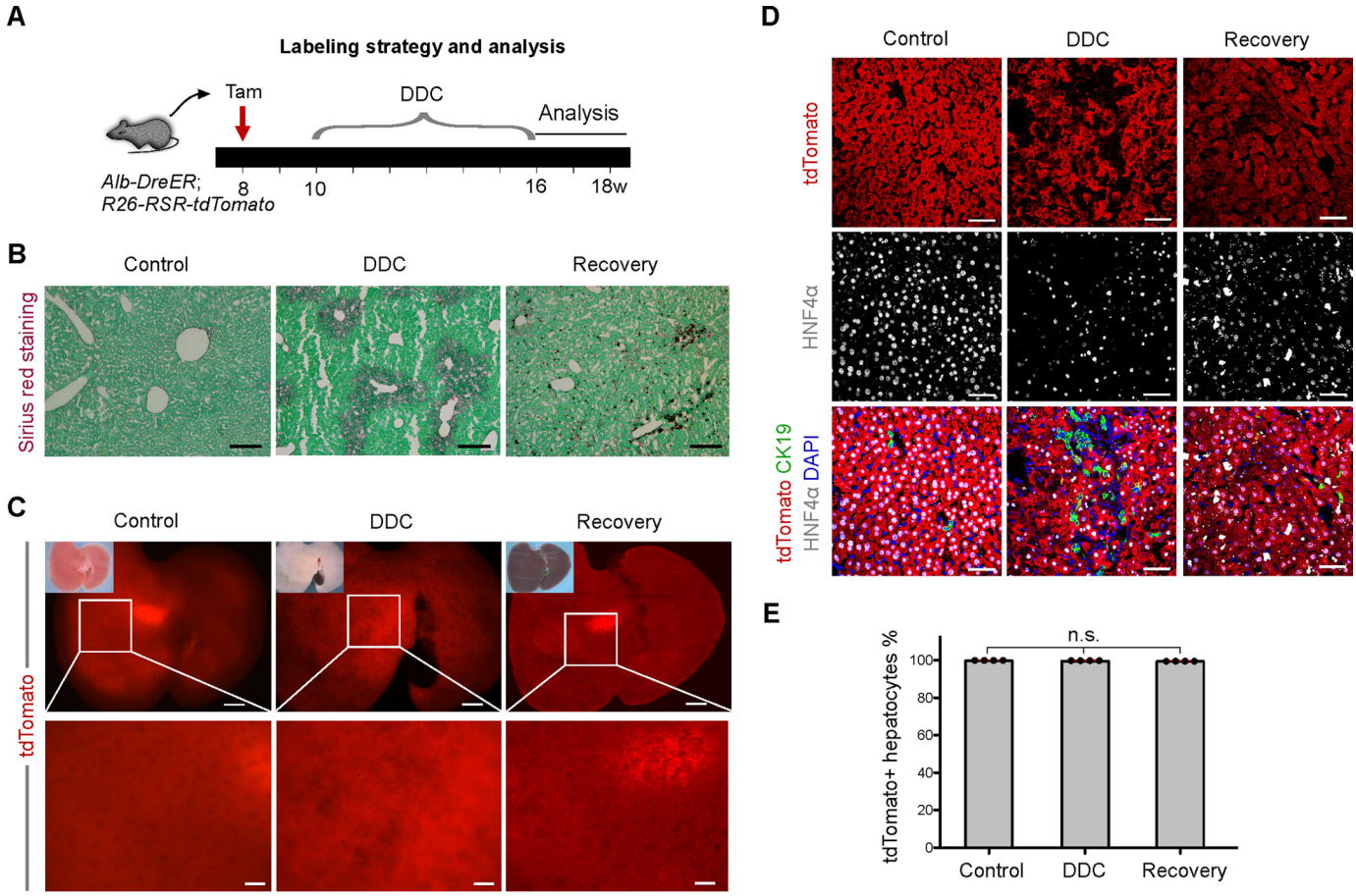

Figure 3. Hepatocytes were derived from pre-existing hepatocytes in DDC-induced liver injury model. *A*, experimental strategy for tamoxifen treatment (*Tam*) and tissue analysis at different time points after Tam. *B*, Sirius red staining of liver sections from Control or DDC-treated mice. *C*, whole-mount fluorescence view of *Alb-DreER;R26-RSR-tdTomato* liver samples. *D*, immunostaining for tdTomato, CK19, and HNF4α on liver sections shows no appreciable change of the efficiency of hepatocyte labeling after injury and recovery. More CK19+ BECs were noted after injury, indicating ductal reaction in DDC-induced liver injury model. *E*, quantification of the percentage of tdTomato+ hepatocytes in different groups. *n.s.*, non-significant; $n = 4$. *Scale bars*: 200 μm in *B*; 1 mm in *C* (*upper*) and 500 μm in *C* (*lower*);100 μm in *D*. *Error bars*, S.E.

hepatocytes (Fig. 2*E*). To exclude that the high labeling efficiency in injured liver is not due to leakiness of DreER, we induced CCl4 in mice that did not receive tamoxifen (*No Tam*). We detected very sparsely labeled hepatocytes (Fig. 2, *F* and *G*), indicating that a high labeling percentage of hepatocytes before and after injury is unlikely due to leakiness of DreER. Quantification of HNF4α$^+$ hepatocytes showed that there is no difference in the percentage of tdTomato$^+$ hepatocytes between control, injury, and recovery groups (99.60 ± 0.11% *versus* 99.38 ± 0.19% *versus* 99.34 ± 0.075%, respectively, $n = 4$, Fig. 2*H*). The percentage of "leaky" tdTomato$^+$ hepatocytes is negligible by quantification (Fig. 2*H*). Taken together, these results demonstrated that almost all hepatocytes in the injured liver are derived from pre-existing hepatocytes. Hepatic progenitor cells, if present, minimally contributed to new hepatocytes after injury.

Hepatocytes are derived from pre-existing hepatocytes after DDC injury

We further examined the contribution of pre-existing hepatocytes to newly generated hepatocytes in DDC-supplemented diet-induced liver damage models. The *Alb-DreER;Rosa26-RSR-tdTomato* mice were induced cholestatic injury with a DDC-containing diet (Fig. 3*A*). Sirius red staining of liver sections showed excessive fibrosis after injury (Fig. 3*B*). Whole-mount epifluorescence images of livers showed no significant drop of tdTomato$^+$ signals in DDC-induced injury group compared with control or recovery groups (Fig. 3*C*). Immunostaining for tdTomato, CK19, and HNF4α showed that a significant ductal reaction in DDC-treated mouse liver and the surviving hepatocytes were almost all tdTomato$^+$ (Fig. 3*D*). Quantification data showed that the percentage of tdTomato$^+$ hepatocytes showed that there is no significant difference between control, DDC, and recovery groups (99.49 ± 0.071% *versus* 99.40 ± 0.096% *versus* 99.41 ± 0.19%, respectively, $n = 4$; Fig. 3*E*). These results indicate that pre-existing hepatocytes are the major source for new hepatocytes in DDC-induced liver injury.

Hepatocytes are derived from pre-existing hepatocytes after CDE injury

We next fed *Alb-DreER;Rosa26-RSR-tdTomato* mice with a CDE diet to induce liver injury (Fig. 4*A*). Sirius red staining showed significant fibrosis after CDE treatment (Fig. 4*B*). Whole-mount fluorescence showed that there is no significant dilution of tdTomato$^+$ signal after injury (Fig. 4*C*). Immuno-

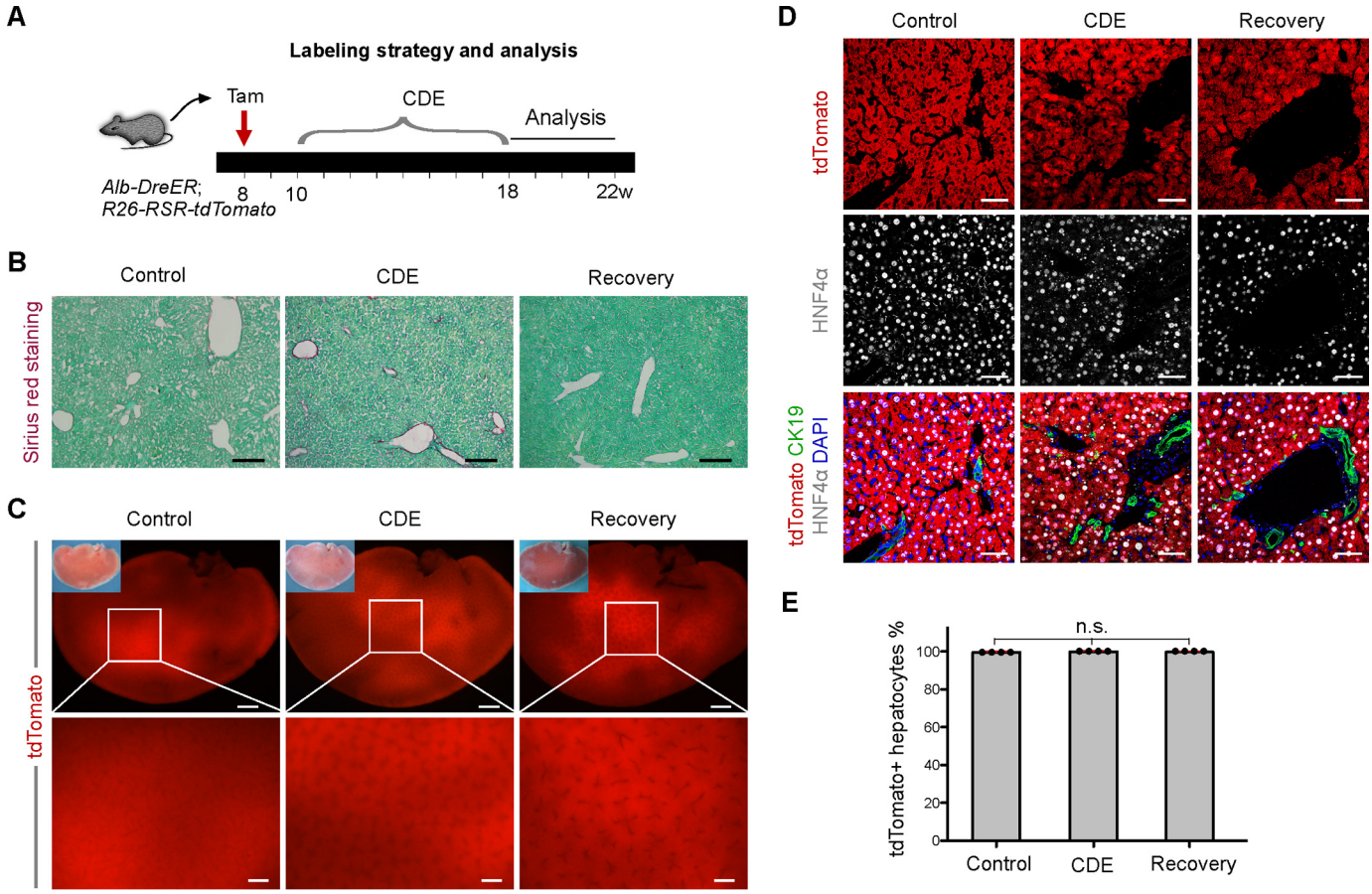

Figure 4. Hepatocytes were derived from pre-existing hepatocytes after CDE injury. *A*, experimental strategy for tamoxifen treatment (*Tam*) and tissue analysis at different time points after Tam. *B*, Sirius red staining of liver sections from Control or CDE-treated mice. *C*, whole-mount fluorescence view of *Alb-DreER;R26-RSR-tdTomato* liver from Control, CDE, or recovery groups. *D*, immunostaining for tdTomato, CK19, and HNF4α on liver sections showed no appreciable change in the frequency of hepatocyte labeling after injury. *E*, quantification of tdTomato+ hepatocytes in different groups. *n.s.*, non-significant; $n = 4$. *Scale bars*, 200 μm in *B*; 1 mm in *C* (*upper*) and 500 μm in *C* (*lower*);100 μm in *D*. *Error bars*, S.E.

staining for tdTomato, CK19, and HNF4α showed an increased number of CK19$^+$ BECs cells after injury, indicating ductal reaction. However, the labeling efficiency of hepatocytes still remains high in CDE liver compared with control or recovery (Fig. 4*D*). Quantification data confirmed that there is no significant difference of the tdTomato$^+$ hepatocyte percentage between control, CDE, and recovery groups (99.58 ± 0.071% *versus* 99.46 ± 0.098% *versus* 99.48 ± 0.23%, respectively, $n = 4$; Fig. 4*E*). Taken together, these data showed that pre-existing hepatocytes are the major source for new hepatocytes after CDE-induced liver injury.

Hepatocytes are derived from pre-existing hepatocytes after α-naphthyl-isothiocyanate (ANIT) injury

Additionally, we fed *Alb-DreER;Rosa26-RSR-tdTomato* mice with an ANIT diet, another cholestatic liver injury model (Fig. 5*A*). Similarly, we used Sirius red staining to confirm the success of liver damage according to inflammatory infiltration and parenchymal necrosis (Fig. 5*B*). A whole-mount fluorescence view of livers showed no appreciable change in tdTomato$^+$ signals from control, ANIT, and recovery groups (Fig. 5*C*). Immunostaining for tdTomato, CK19, and HNF4α showed that although there is increased CK19$^+$ BECs during ductal reaction, efficiency of labeled hepatocytes remains similar between these three groups (Fig. 5*D*). Quantification data showed that there is no significant difference of the percentage of tdTomato$^+$ hepatocytes between control, ANIT, and recovery groups (99.61 ± 0.081% *versus* 99.56 ± 0.14% *versus* 99.47 ± 0.18%, respectively, $n = 4$; Fig. 5*E*). Taken together, these data demonstrated that pre-existing hepatocytes are the major origin for new hepatocytes in ANIT-induced liver injury model.

Hepatocytes are derived from pre-existing hepatocytes after partial hepatectomy (PHx)

As a control, we performed mice surgeries to test the changes of adult hepatocytes. We designed 2/3 PHx using *Alb-IRES-DreER;Rosa26-RSR-tdTomato* mice and collected livers at different times (Fig. 6*A*). Sirius red staining showed that there was no fibrosis after PHx, indicating that the surgery is successful, and no other additional injuries were induced (Fig. 6*B*). Collecting livers from PHx mice proved the size became much larger than sham mice, demonstrating that the extent of hepatocyte proliferation is directly proportional to the amount of resected liver tissue (Fig. 6*C*). Immunostaining for tdTomato, CK19, and HNF4α showed that there is also no change in the tdTomato labeling index in both the short-time and long-time recovery (Fig. 6*D*). Quantification data showed that there is no significant difference of the percentage of tdTomato$^+$ hepatocytes

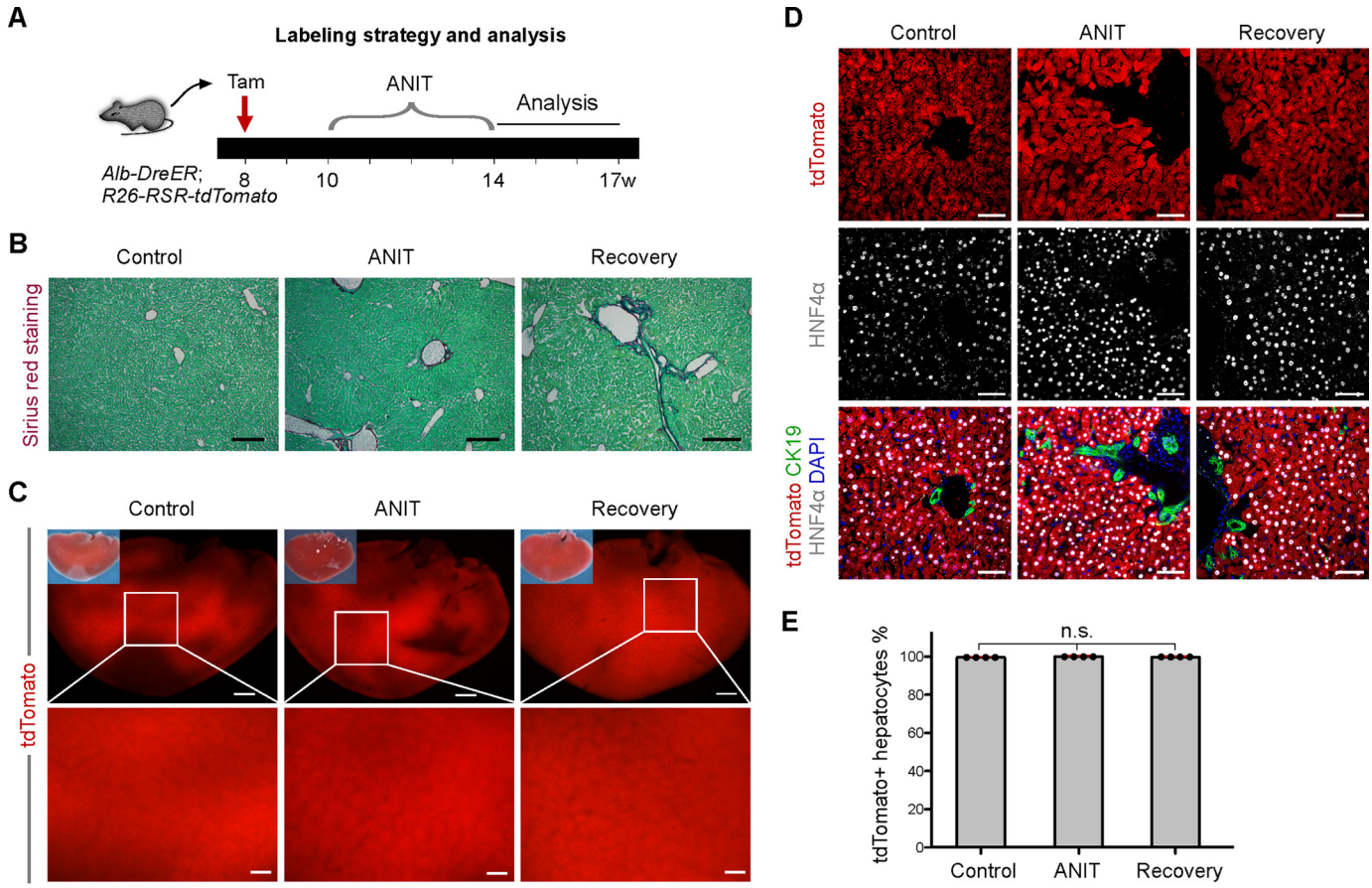

Figure 5. Hepatocytes were derived from pre-existing hepatocytes after ANIT injury. *A*, experimental strategy for tamoxifen treatment (*Tam*) and tissue analysis at different time points after Tam. *B*, Sirius red staining of liver sections from Control or ANIT-treated mice. *C*, whole-mount fluorescence view of *Alb-DreER;R26-RSR-tdTomato* liver at Control or ANIT treatment. *D*, immunostaining for tdTomato, CK19, and HNF4α on liver sections. *E*, quantification of tdTomato+ hepatocytes in different groups. *n.s.*, non-significant; $n = 4$. *Scale bars*, 200 μm in *B*; 1 mm in *C* (*upper*) and 500 μm in *C* (*lower*);100 μm in *D*. *Error bars*, S.E.

between sham and recovery groups (99.55 ± 0.21% *versus* 99.46 ± 0.25% *versus* 99.52 ± 0.18%, respectively, $n = 4$; Fig. 6*E*).

Hepatocytes are derived from pre-existing hepatocytes after bile-duct ligation (BDL) injury

Next, we operated on the *Alb-DreER;Rosa26-RSR-tdTomato* mice with bile BDL (Fig. 7*A*). Sirius red staining showed that there was serious fibrosis after BDL, indicating that the surgery is performed successfully (Fig. 7*B*). Collecting livers from sham mice or BDL-treated mice proved the severe bile duct injury (Fig. 7*C*). Immunostaining for tdTomato, CK19, and HNF4α showed that there is also no change in the tdTomato labeling percentage after mice recovery (Fig. 7*D*). Quantification data showed that there is no significant difference of the percentage of tdTomato$^+$ hepatocytes between sham and recovery groups (99.58 ± 0.14% *versus* 99.60 ± 0.089%, respectively, $n = 4$; Fig. 7*E*).

Discussion

In this study we used lineage tracing approaches to test the source of hepatocytes after toxin- or surgery-induced liver damage and repair/regeneration. We genetically labeled albumin-expressing hepatocytes with high efficiency and specificity and found that there was no detectable change in labeling proportion with six mentioned types of injury in our research. Almost all hepatocytes were labeled after injury, similar to those labeled before injury. Taken together, our genetic lineage tracing data suggest that non-hepatocyte populations are unable to contribute significantly to hepatocyte neogenesis during liver repair and regeneration.

Recent findings have recrudesced a long-term debate about whether hepatocytes or facultative stem cells, also known as "oval cells" or "atypical ductal cells," are the main source of new hepatocytes in liver regeneration. It has been proposed that atypical ductal cells are special stem cells that are based on *in vitro* studies and cellular transplantation assays (4, 20). Overall, *in vitro* and cell-transplantation studies are able to reflect the potential of a certain type of cell under the established experimental conditions, whereas lineage-tracing studies prefer to provide insights into cell fate *in vivo* without manipulating cells by isolation, culture, and transplantation.

Indeed, the stem-cell paradigm prevails in many adult tissues. In the mammalian liver the stem-cell paradigm has become a heated debate based on controversial lineage studies, as stem cells are reported to differentiate into new hepatocytes after injury. Genetic lineage-tracing studies based on Cre-loxP systems (Hnf1β, Sox9, Osteopontin, etc.) supported that resident liver progenitor cells contribute to new hepatocytes after

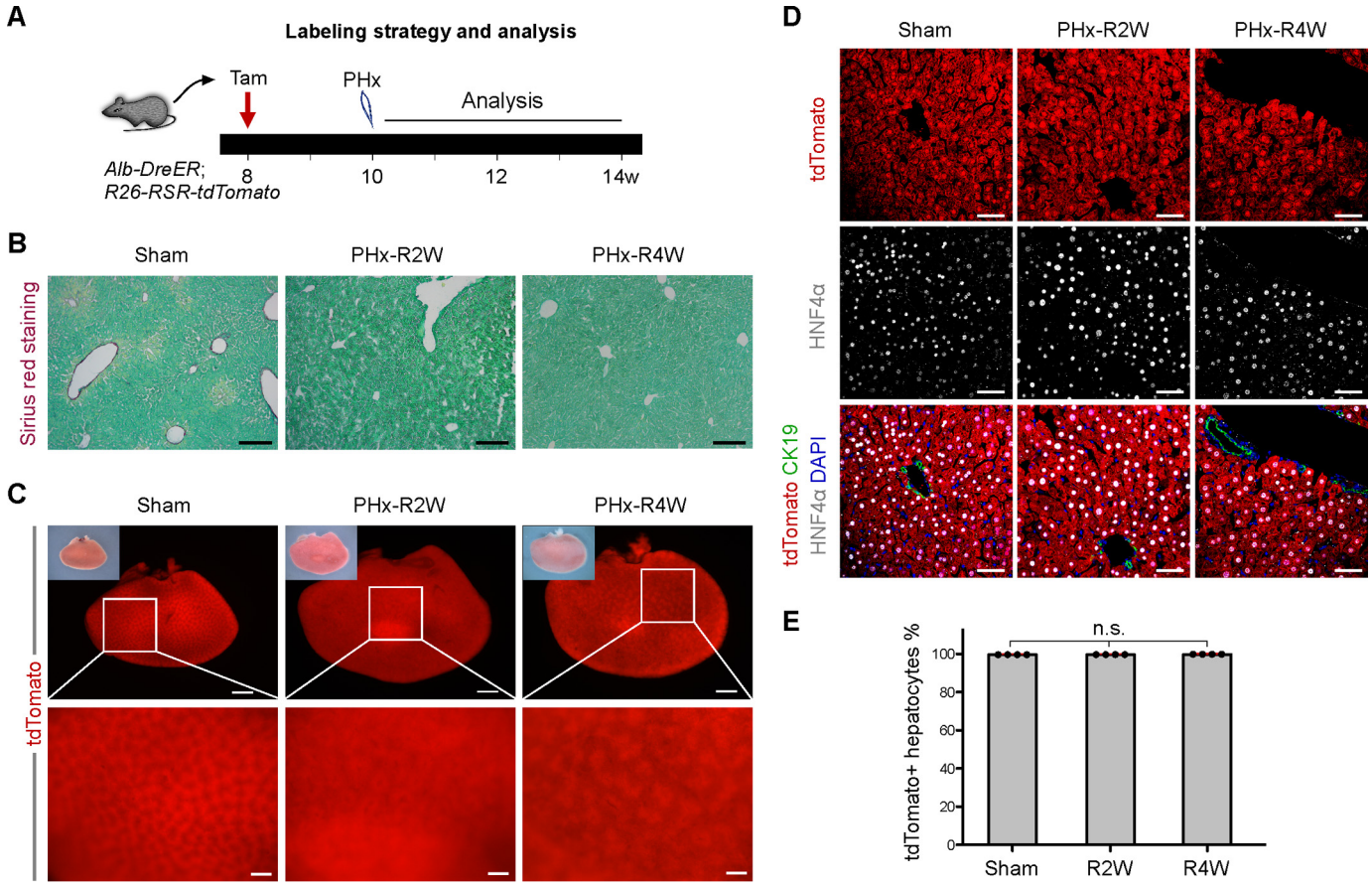

Figure 6. Hepatocytes were derived from pre-existing hepatocytes after PHx injury. *A*, experimental strategy for tamoxifen treatment (*Tam*) and tissue analysis at different time points after Tam. *B*, Sirius red staining of liver sections from Sham or PHx-injured mice. *R2W*, recovery 2 weeks after PHx; *R4W*, recovery 4 weeks after PHx. *C*, whole-mount fluorescence view of *Alb-DreER;R26-RSR-tdTomato* liver at Sham or PHx injury. *D*, immunostaining for tdTomato, CK19, and HNF4α on liver sections shows liver histology after PHx injuries with no appreciable change in the frequency of hepatocyte labeling. *E*, quantification of tdTomato+ hepatocytes in different groups. *n.s.*, non-significant; $n = 4$. *Scale bars*: 200 μm in *B*; 1 mm in *C* (*upper*) and 500 μm in *C* (*lower*); 100 μm in *D*. *Error bars*, S.E.

injury and during liver regeneration (3, 7, 21). Recent lineage-tracing studies suggested that adult hepatocytes are generated by self-duplication rather than stem cell differentiation (10, 22). Almost all of these previous studies used adeno-associated virus (AAV) for expression of Cre recombinase in hepatocytes (10, 22). A popular *in vivo* reprogramming strategy is delivery of the transcription factors to the targeted cells, which is thought efficient and safe (23, 24). The exploration of used delivery vectors is particularly important. Different AAV capsids have various transducing efficiency for cell types. Most researchers used a replication-incompetent, recombinant adeno-associated virus serotype 2/8 expressing Cre recombinase driven by the hepatocyte-specific promoter (thyroid hormone-binding globulin, AAV8-TBG-Cre) (10). This transduction is highly specific (6, 25). Moreover, this labeling is efficient, as the majority of hepatocytes are genetically marked when mice are infected (10), with no labeling of non-hepatocytes (6). However, the efficiency of this labeling method depends on the doses of vectors that are not controlled very well (26). Meanwhile, the duration of virus-mediated labeling of hepatocytes was unknown. It is also unclear if excessive virus would have any positive or negative influence on the proliferation or function of hepatocytes. The effect of liver injury models on the labeling efficiency and specificity induced by AAVs was also obscure. In our study we used genetic lineage labeling tools *Alb-DreER* to efficiently label almost all of the hepatocytes to trace the changes of hepatocyte labeling after liver injuries. The pulse-and-chase strategy showed no significant change of hepatocyte labeling by different injury models, suggesting minimal, if any, contribution of facultative stem cells to new hepatocytes. This is by far the first knock-in model to systematically address if pre-existing hepatocytes are the main, if not exclusive, source of new hepatocytes after injury. Our data support the view that new adult hepatocytes arise from pre-existing hepatocytes not only after partial hepatectomy and bile-duct ligation but also in the setting of toxin injuries as well, which is consistent with previous reports (10, 27). As hepatocytes have the remarkable ability of proliferation (28) and can also differentiate into biliary cells on injury (5, 6, 29), hepatocytes themselves appear to constitute the facultative progenitor cell compartment of the liver.

In addition, the novel tool we generated is also useful for a more sophisticated study of different populations, as Cre-loxP and Dre-rox are two orthogonal systems that could be used to genetically target two different cell populations simultaneously *in vivo*. Furthermore, the precision of the broadly using Cre-loxP system would be improved when it is combined with the Dre-rox system for genetic targeting. Recently, we used the intersectional genetics based on both Cre-loxP and Dre-rox

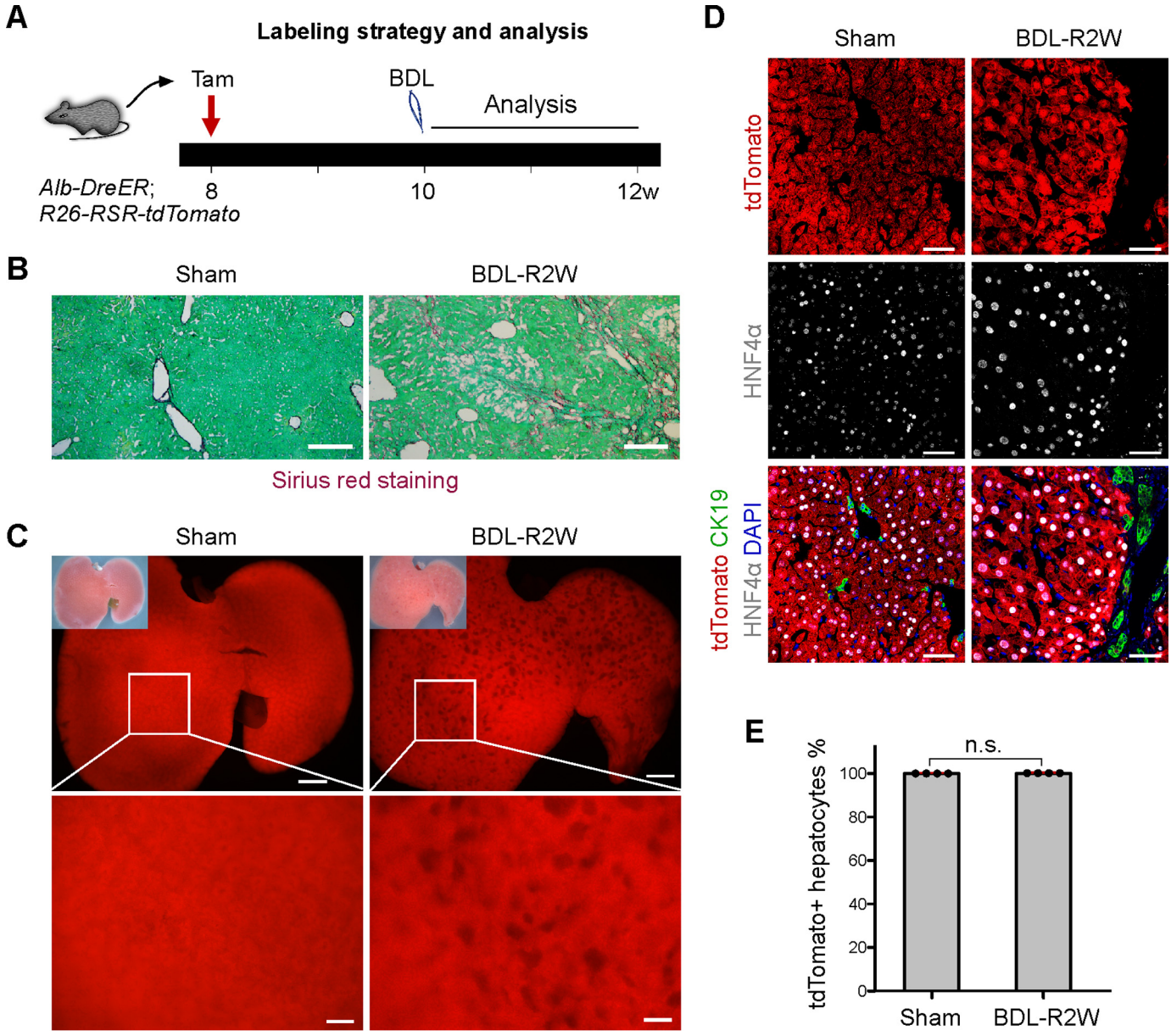

Figure 7. Hepatocytes were derived from pre-existing hepatocytes after BDL injury. *A*, experimental strategy for tamoxifen treatment (*Tam*) and tissue analysis at different time points after Tam. *B*, Sirius red staining of liver sections from Sham or BDL-injured mice. *R2W*, recovery 2 weeks after BDL. *C*, whole-mount fluorescence view of *Alb-DreER;R26-RSR-tdTomato* liver at Sham or BDL injury. *D*, immunostaining for tdTomato, CK19, and HNF4α on liver sections shows liver histology after BDL injuries with no appreciable change in the frequency of hepatocyte labeling. *E*, quantification of tdTomato+ hepatocytes in different groups. *n.s.*, non-significant; $n = 4$. *Scale bars*: 200 μm in B; 1 mm in *C* (*upper*) and 500 μm in *C* (*lower*);100 μm in *D*. *Error bars*, S.E.

systems and found that some liver vasculature originates from endocardial cells in development (18), indicating the unique property of Dre-rox system of integrating into the widely used Cre-loxP system. Likewise, one quick application of *Alb-DreER* in a liver study, for example, is to combine it with *Sox9-CreER* to more precisely trace $Sox9^+Alb^+$-hybrid hepatocytes (30) without targeting of $Sox9^+Alb^-$ biliary epithelial cells. Therefore, the *Alb-DreER* tool generated in this study not only resolves the previous controversy by an *in vivo* genetic study without depending on excessive virus infection, but it also provides an alternative new mouse tool to the field, facilitating more precise genetic manipulation of hepatocytes *in vivo* in the future studies.

Experimental procedures

Mice

All animal studies were carried out in accordance with the guidelines of the Institutional Animal Care and Use Committee (IACUC) of the Institute for Nutritional Sciences, Shanghai Institutes for Biological Sciences, Chinese Academy of Science. Mice were maintained on a C129/C57BL6/J;ICR mixed background. *Alb-DreER* was generated by CRISPR/Cas9 through homologous recombination. A cDNA encoding IRES-$DreER^{T2}$ was inserted in-frame with the translational termination codon of the albumin gene. The chimeric mice positive for targeted ES cells were germ line transferred to F1 generation and bred on a

C57BL/6;ICR background. *Ai66* (*Rosa26-Rox-Stop-Rox-LoxP-Stop-LoxP-tdTomato*) was reported previously (31). The *Rosa26-Rox-Stop-Rox-tdTomato* (*Rosa26-RSR-tdTomato*) mouse line was generated by crossing *ACTB-Cre* (32) with *Ai66* to excise the *LoxP*-flanked *Stop* cassette, and *ACTB-Cre* was not passaged to the subsequent generation. *Rosa26-RSR-tdTomato* (16, 17) was responsive to Dre but not Cre recombinase. The *Alb-DreER* line was generated by Shanghai Biomodel Organism Science and Technology Development Co., Ltd. All experimental mice were maintained on a C57BL/6;ICR background. Tamoxifen (Sigma, T5648) was dissolved in corn oil and administered to mice at the indicated time. Adult mice received 0.1–0.2 mg of tamoxifen/g of mouse body weight by oral gavage.

Genomic PCR

Genomic DNA was prepared from mouse toes or tail. Tissues were lysed by incubation with proteinase K overnight at 55 °C followed by centrifugation at maximum speed for 8 min to obtain supernatant with genomic DNA. DNA was precipitated by adding isopropyl alcohol and washed in 70% ethanol. All mice were genotyped with specific primers that distinguish knock-in allele from wild-type allele. For the *Rosa26-RSR-tdTomato* line, primers 5′-ACGGGTGTTGGGTCGTTTGTTC-3′ and 5′-TTCTTGTAATCGGGGATGTCGGCG-3′ were used to detect the TDTOMATO-positive allele, and 5′-AAGGGAGCTGCAGTGGAGTA-3′ and 5′-CCGAA AATCTGTGGGAAGTC-3′ were used to detect the wild-type allele. For the *Alb-DreER* line, primers 5′-TTCAGGGTCCAAACCTTGTCAC-3′ and 5′-ACTCCTTGCCGATGTTCCTCAG-3′ were used to detect the $DreER^{T2}$ positive allele, and 5′-TTCAGGGTCCAAACCTTGTCAC-3′ and 5′-GAGCAAAACCAGGGCTAACTCC-3′ were used to detect the wild-type allele.

Injury model

For the CCl_4-induced chronic injury model, CCl_4 was dissolved at 1:3 in corn oil and injected intraperitoneally at a dose of 4 μl/g body weight every 3 days for 10 times (22). Mice were given 0.1% wt/wt DDC (Sigma) PMI Mouse Diet #5015 (Harlan Teklad) for 6 weeks, at which point the diet was changed to regular chow for 2 weeks to allow mice to recover. A choline-deficient diet (FBSH China) supplemented with 0.15% ethionine drinking water (Sigma, E5139) was administered for 8 weeks followed by 4 weeks of recovery. ANIT (dissolved in oil, 60 mg/kg) was administered intraperitoneally every 3 days for 10 times followed by 3–4 weeks of recovery. PHx and BDL were performed as described previously (19).

Immunostaining

Immunostaining was performed according to protocols described previously (33). Tissues were dissected in PBS and fixed in 4% paraformaldehyde (Sigma) at 4 °C for 1 h. Afterward, tissues were washed in PBS and dehydrated in 30% sucrose overnight at 4 °C and embedded in OCT (Sakura). 10-μm cryosections were obtained and air-dried afterward at room temperature. For staining, dried sections were washed in PBS and then blocked with 5% normal donkey serum (Jackson ImmunoResearch) and 0.1% Triton X-100 in PBS for 30 min at room temperature. Sections were incubated with the primary antibodies overnight at 4 °C. The following antibodies were used: tdTomato (Rockland, 600-401-379, 1:200), cytokeratin 19 (Developmental Studies Hybridoma Bank, TROMA-III, 1:100), HNF4a (Santa Cruz, sc-6556, 1:100), VE-cadherin (R&D, AF1002, 1:100), Desmin (R & D, AF3844, 1:100), PDGFRα (R&D, AF1062, 1:100), EpCAM (Abcam, ab92383, 1:100), Sox9 (Millipore, AB5535, 1:100), αSMA (Sigma, F3777, 1:100). Signals were developed with Alexa fluorescence antibodies (Invitrogen), and nuclei were stained with 4′6-diamidino-2-phenylindole (DAPI, Vector Laboratories). Immunostaining images were acquired by an Olympus fluorescence microscope (BX53), a Zeiss stereomicroscope (AXIO Zoom. V16), a Zeiss confocal laser scanning microscope (LSM510), and an Olympus confocal microscope (FV1200).

Sirius red staining

Sirius red staining was aimed to assess fibrotic tissue formation after chronic injury and was performed as described previously (34). Cryosections were fixed in 4% paraformaldehyde for 15 min, then washed in PBS for 15 min and fixed overnight in Bouins solution (5% acetic acid, 9% formaldehyde, 0.9% picric acid). Subsequently, sections were stained with 0.1% Fast Green (Fisher) for 3 min and incubated in 1% acetic acid for 1 min followed by incubation with 0.1% Sirius red (Sigma) for 2 min. Sections were rinsed with tap water before incubation into the staining solution. Slides were dehydrated in 100% ethanol twice, cleared in xylene, and mounted with resinous medium. Images were obtained on an Olympus microscope (BX53).

Statistics

Data for two groups were analyzed by a two-tailed unpaired Student's *t* test, whereas comparison between more than two groups was performed using a analysis of variance followed by Tukey's multiple comparison test. Significance was accepted when $p < 0.05$. All data are presented as the mean ± S.E.

Author contributions—Y. W. and B. Z. designed the study, performed the experiments, and analyzed the data. X. H., L. H., W. P., Yan Li, Q. L., Yi Li, L. Z., W. Y., H. Z., and Y.Z. bred the mice, performed the experiments, and provided intellectual input. B. Z. conceived and supervised the study, analyzed the data, and wrote the manuscript.

Acknowledgments—We thank H. Zeng for sharing mice lines and K. Anastassiadis for valuable suggestions and insightful advice on this study.

References

1. Grompe, M. (2014) Liver stem cells, where art thou? *Cell Stem Cell* **15,** 257–258
2. Miyajima, A., Tanaka, M., and Itoh, T. (2014) Stem/progenitor cells in liver development, homeostasis, regeneration, and reprogramming. *Cell Stem Cell* **14,** 561–574
3. Español-Suñer, R., Carpentier, R., Van Hul, N., Legry, V., Achouri, Y., Cordi, S., Jacquemin, P., Lemaigre, F., and Leclercq, I. A. (2012) Liver progenitor cells yield functional hepatocytes in response to chronic liver injury in mice. *Gastroenterology* **143,** 1564–1575 e1567
4. Huch, M., Dorrell, C., Boj, S. F., van Es, J. H., Li, V. S., van de Wetering, M., Sato, T., Hamer, K., Sasaki, N., Finegold, M. J., Haft, A., Vries, R. G.,

Grompe, M., and Clevers, H. (2013) *In vitro* expansion of single Lgr5+ liver stem cells induced by Wnt-driven regeneration. *Nature* **494,** 247–250
5. Tanimizu, N., Nishikawa, Y., Ichinohe, N., Akiyama, H., and Mitaka, T. (2014) Sry HMG box protein 9-positive (Sox9+) epithelial cell adhesion molecule-negative (EpCAM-) biphenotypic cells derived from hepatocytes are involved in mouse liver regeneration. *J. Biol. Chem.* **289,** 7589–7598
6. Yanger, K., Zong, Y., Maggs, L. R., Shapira, S. N., Maddipati, R., Aiello, N. M., Thung, S. N., Wells, R. G., Greenbaum, L. E., and Stanger, B. Z. (2013) Robust cellular reprogramming occurs spontaneously during liver regeneration. *Genes Dev.* **27,** 719–724
7. Rodrigo-Torres, D., Affò, S., Coll, M., Morales-Ibanez, O., Millán, C., Blaya, D., Alvarez-Guaita, A., Rentero, C., Lozano, J. J., Maestro, M. A., Solar, M., Arroyo, V., Caballería, J., van Grunsven, L. A., *et al.* (2014) The biliary epithelium gives rise to liver progenitor cells. *Hepatology* **60,** 1367–1377
8. Schaub, J. R., Malato, Y., Gormond, C., and Willenbring, H. (2014) Evidence against a stem cell origin of new hepatocytes in a common mouse model of chronic liver injury. *Cell Rep.* **8,** 933–939
9. Tarlow, B. D., Finegold, M. J., and Grompe, M. (2014) Clonal tracing of Sox9+ liver progenitors in mouse oval cell injury. *Hepatology* **60,** 278–289
10. Yanger, K., Knigin, D., Zong, Y., Maggs, L., Gu, G., Akiyama, H., Pikarsky, E., and Stanger, B. Z. (2014) Adult hepatocytes are generated by self-duplication rather than stem cell differentiation. *Cell Stem Cell* **15,** 340–349
11. Carpentier, R., Suñer, R. E., van Hul, N., Kopp, J. L., Beaudry, J. B., Cordi, S., Antoniou, A., Raynaud, P., Lepreux, S., Jacquemin, P., Leclercq, I. A., Sander, M., and Lemaigre, F. P. (2011) Embryonic ductal plate cells give rise to cholangiocytes, periportal hepatocytes, and adult liver progenitor cells. *Gastroenterology* **141,** 1432–1438
12. Isse, K., Lesniak, A., Grama, K., Maier, J., Specht, S., Castillo-Rama, M., Lunz, J., Roysam, B., Michalopoulos, G., and Demetris, A. J. (2013) Preexisting epithelial diversity in normal human livers: a tissue-tethered cytometric analysis in portal/periportal epithelial cells. *Hepatology* **57,** 1632–1643
13. Arroyo, V., García-Martinez, R., and Salvatella, X. (2014) Human serum albumin, systemic inflammation, and cirrhosis. *J. Hepatol* **61,** 396–407
14. Garcia-Martinez, R., Caraceni, P., Bernardi, M., Gines, P., Arroyo, V., and Jalan, R. (2013) Albumin: pathophysiologic basis of its role in the treatment of cirrhosis and its complications. *Hepatology* **58,** 1836–1846
15. Kubota, H., and Reid, L. M. (2000) Clonogenic hepatoblasts, common precursors for hepatocytic and biliary lineages, are lacking classical major histocompatibility complex class I antigen. *Proc. Natl. Acad. Sci. U.S.A.* **97,** 12132–12137
16. Zhang, H., Pu, W., Li, G., Huang, X., He, L., Tian, X., Liu, Q., Zhang, L., Wu, S. M., Sucov, H. M., and Zhou, B. (2016) Endocardium minimally contributes to coronary endothelium in the embryonic ventricular free walls. *Circ. Res.* **118,** 1880–1893
17. Zhang, H., Pu, W., Liu, Q., He, L., Huang, X., Tian, X., Zhang, L., Nie, Y., Hu, S., Lui, K. O., and Zhou, B. (2016) Endocardium contributes to cardiac fat. *Circ. Res.* **118,** 254–265
18. Zhang, H., Pu, W., Tian, X., Huang, X., He, L., Liu, Q., Li, Y., Zhang, L., He, L., Liu, K., Gillich, A., and Zhou, B. (2016) Genetic lineage tracing identifies endocardial origin of liver vasculature. *Nat. Genet.* **48,** 537–543
19. Pu, W., Zhang, H., Huang, X., Tian, X., He, L., Wang, Y., Zhang, L., Liu, Q., Li, Y., Li, Y., Zhao, H., Liu, K., Lu, J., *et al.* (2016) Mfsd2a+ hepatocytes repopulate the liver during injury and regeneration. *Nat. Commun.* **7,** 13369
20. Shin, S., Walton, G., Aoki, R., Brondell, K., Schug, J., Fox, A., Smirnova, O., Dorrell, C., Erker, L., Chu, A. S., Wells, R. G., Grompe, M., Greenbaum, L. E., and Kaestner, K. H. (2011) Foxl1-Cre-marked adult hepatic progenitors have clonogenic and bilineage differentiation potential. *Genes Dev.* **25,** 1185–1192
21. Furuyama, K., Kawaguchi, Y., Akiyama, H., Horiguchi, M., Kodama, S., Kuhara, T., Hosokawa, S., Elbahrawy, A., Soeda, T., Koizumi, M., Masui, T., Kawaguchi, M., Takaori, K., Doi, R., Nishi, E., *et al.* (2011) Continuous cell supply from a Sox9-expressing progenitor zone in adult liver, exocrine pancreas and intestine. *Nat. Genet.* **43,** 34–41
22. Malato, Y., Naqvi, S., Schürmann, N., Ng, R., Wang, B., Zape, J., Kay, M. A., Grimm, D., and Willenbring, H. (2011) Fate tracing of mature hepatocytes in mouse liver homeostasis and regeneration. *J. Clin. Invest.* **121,** 4850–4860
23. Addis, R. C., and Epstein, J. A. (2013) Induced regeneration: the progress and promise of direct reprogramming for heart repair. *Nat. Med.* **19,** 829–836
24. Heinrich, C., Spagnoli, F. M., and Berninger, B. (2015) *In vivo* reprogramming for tissue repair. *Nat. Cell Biol.* **17,** 204–211
25. Wang, L., Wang, H., Bell, P., McCarter, R. J., He, J., Calcedo, R., Vandenberghe, L. H., Morizono, H., Batshaw, M. L., and Wilson, J. M. (2010) Systematic evaluation of AAV vectors for liver directed gene transfer in murine models. *Mol. Ther.* **18,** 118–125
26. Rezvani, M., Español-Suñer, R., Malato, Y., Dumont, L., Grimm, A. A., Kienle, E., Bindman, J. G., Wiedtke, E., Hsu, B. Y., Naqvi, S. J., Schwabe, R. F., Corvera, C. U., Grimm, D., and Willenbring, H. (2016) *In vivo* hepatic reprogramming of myofibroblasts with AAV vectors as a therapeutic strategy for liver fibrosis. *Cell Stem Cell* **18,** 809–816
27. Tarlow, B. D., Pelz, C., Naugler, W. E., Wakefield, L., Wilson, E. M., Finegold, M. J., and Grompe, M. (2014) Bipotential adult liver progenitors are derived from chronically injured mature hepatocytes. *Cell Stem Cell* **15,** 605–618
28. Overturf, K., al-Dhalimy, M., Ou, C. N., Finegold, M., and Grompe, M. (1997) Serial transplantation reveals the stem-cell-like regenerative potential of adult mouse hepatocytes. *Am. J. Pathol.* **151,** 1273–1280
29. Sekiya, S., and Suzuki, A. (2014) Hepatocytes, rather than cholangiocytes, can be the major source of primitive ductules in the chronically injured mouse liver. *Am. J. Pathol.* **184,** 1468–1478
30. Font-Burgada, J., Shalapour, S., Ramaswamy, S., Hsueh, B., Rossell, D., Umemura, A., Taniguchi, K., Nakagawa, H., Valasek, M. A., Ye, L., Kopp, J. L., Sander, M., Carter, H., Deisseroth, K., Verma, I. M., and Karin, M. (2015) Hybrid periportal hepatocytes regenerate the injured liver without giving rise to cancer. *Cell* **162,** 766–779
31. Madisen, L., Garner, A. R., Shimaoka, D., Chuong, A. S., Klapoetke, N. C., Li, L., van der Bourg, A., Niino, Y., Egolf, L., Monetti, C., Gu, H., Mills, M., Cheng, A., Tasic, B., Nguyen, T. N., *et al.* (2015) Transgenic mice for intersectional targeting of neural sensors and effectors with high specificity and performance. *Neuron* **85,** 942–958
32. Lewandoski, M., Meyers, E. N., and Martin, G. R. (1997) Analysis of Fgf8 gene function in vertebrate development. *Cold Spring Harb. Symp. Quant. Biol.* **62,** 159–168
33. Liu, Q., Yang, R., Huang, X., Zhang, H., He, L., Zhang, L., Tian, X., Nie, Y., Hu, S., Yan, Y., Zhang, L., Qiao, Z., Wang, Q. D., Lui, K. O., and Zhou, B. (2016) Genetic lineage tracing identifies *in situ* kit-expressing cardiomyocytes. *Cell Res.* **26,** 119–130
34. He, L., Liu, Q., Hu, T., Huang, X., Zhang, H., Tian, X., Yan, Y., Wang, L., Huang, Y., Miquerol, L., Wythe, J. D., and Zhou, B. (2016) Genetic lineage tracing discloses arteriogenesis as the main mechanism for collateral growth in the mouse heart. *Cardiovasc. Res.* **109,** 419–430